



Milad Heidari-Koochi ^a, Ioannis K. Karathanassis ^a, Phoevos Koukouvinis ^a, Jin Wang ^b, Manolis Gavaises ^a
^a SMCSE, City, University of London, London, UK
^b Advanced Photon Source, Argonne National Laboratory, Lemont, USA

1. Introduction

The emergence, development and collapse of cavitation bubbles can profoundly influence both natural and man-made flow processes. Appropriate treatment of cavitation can improve the quality and performance of a wide range of applications from biomedical such as focused ultrasound devices and mechanical heart valves [1,2], to industrial applications such as design of turbomachinery blades, rocket engines, and fuel injection systems [3-6]. The present work is focused on the inertial cavitation arising in high-velocity, turbulent liquid flow stemming in a large replica of an injection where a general categorisation of cavitation regimes demonstrates a distinct transient nature in two forms of cloud and vortical cavitation. Two X-ray imaging techniques, i.e. X-ray Phase Contrast Imaging and X-ray Absorption, have been employed to provide both qualitative and quantitative measurements of the in-nozzle two-phase flow.

3. X-ray Phase Contrast Imaging (XPCI)

In XPCI method, the phase shift in the attenuation of an X-ray beam can be explicitly correlated to the imaginary part of the material refractive index which occurs due to the X-ray Compton and Rayleigh scatterings. As a result, fine features of the two-phase flow are highlighted. A set of 10000 twelve-bit greyscale radiographs were acquired at each panel of the irradiated test model to study the morphology and dynamics of the cavitating flow within the orifice. Fig. 2 demonstrates various techniques utilised sequentially to distinguish between the vaporous structures and the surrounding liquid phase. As illustrated in the mean vapour probability contour plots (Fig. 3), for low needle lifts a longitudinal vortical cavity appears and extends to the orifice outlet, while on the contrary, for high lifts the entire cavity trailing edge is wider and a cloud shedding process is in place.

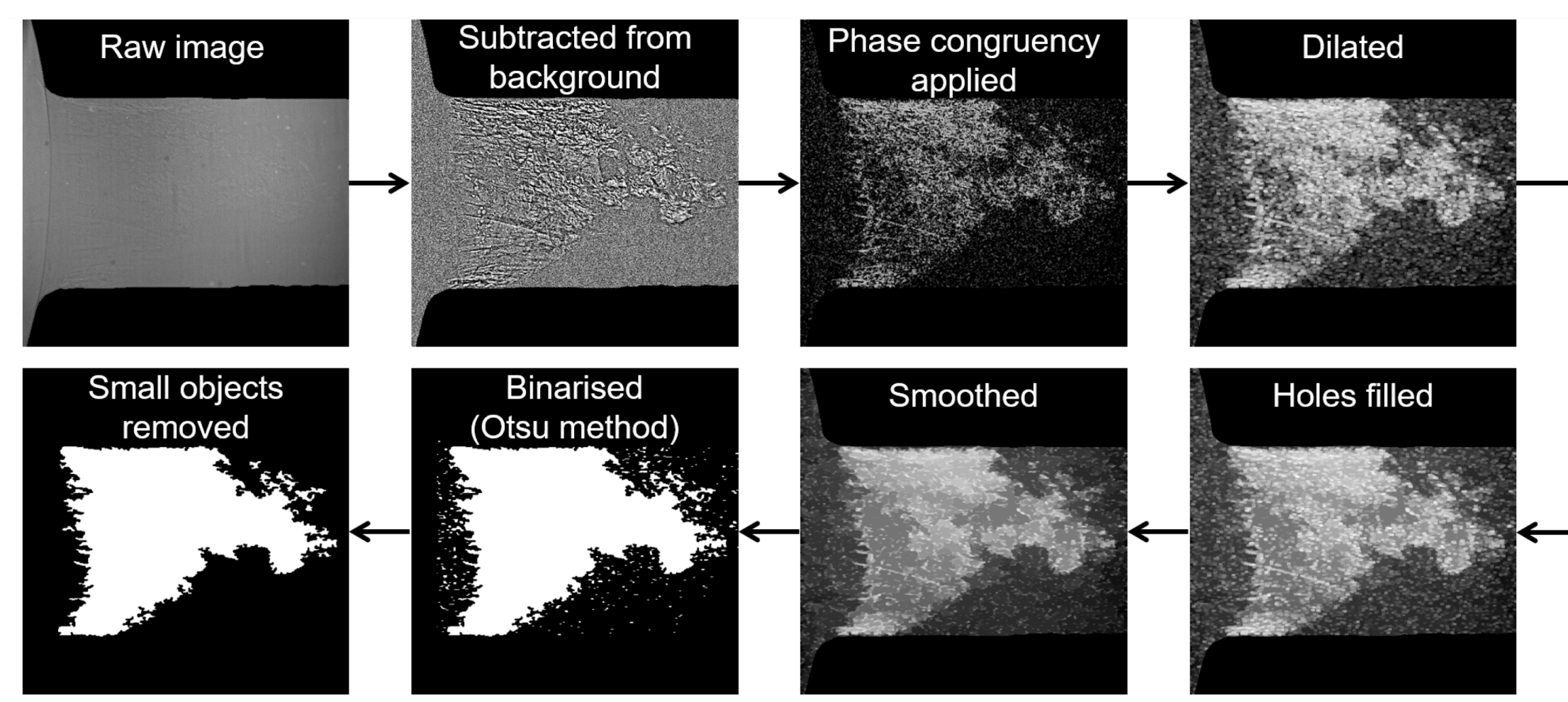


Figure 2. Post processing technique employed for XPCI experiment at the second panel.

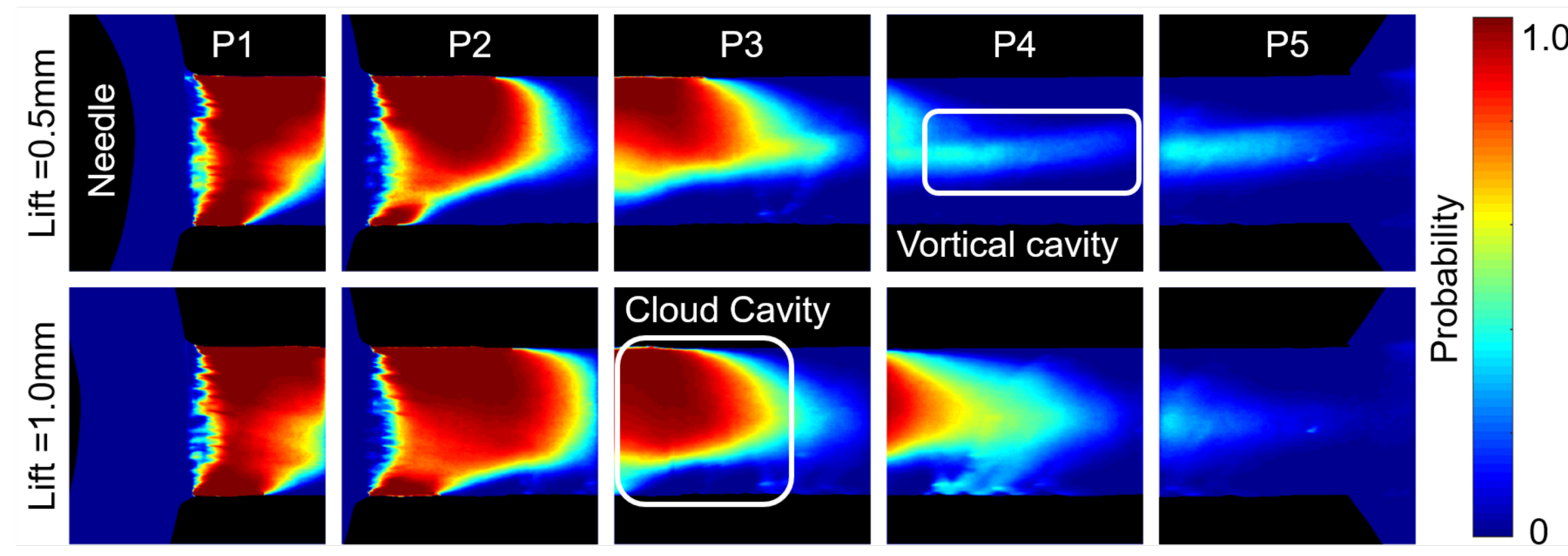


Figure 3. Contour plots of the mean vapour probability for CN=4. Flow is from left to right.

4. X-ray Absorption

The presence of cavitation structures in the flow path of the irradiated nozzle results in an increase of the percentage of irradiation, I , reaching the scintillator compared to the respective I_0 for the case where the nozzle is occupied solely by liquid. Postulating that beam attenuation occurs only due to absorption in the irradiated material layers, the accumulated projected (line-of-sight) vapour thickness can be calculated through the Beer-Lambert law: $I/I_0 = e^{-\mu \lambda}$

where μ is the attenuation coefficient of the liquid medium (the respective of vapour corresponds to negligibly small values) and λ is the vapour mean path (thickness). Figs. 4 & 5 represent the processing technique employed to derive quantitative information and the resulting contour plots of the mean vapour path acquired from 5000 radiographs respectively.

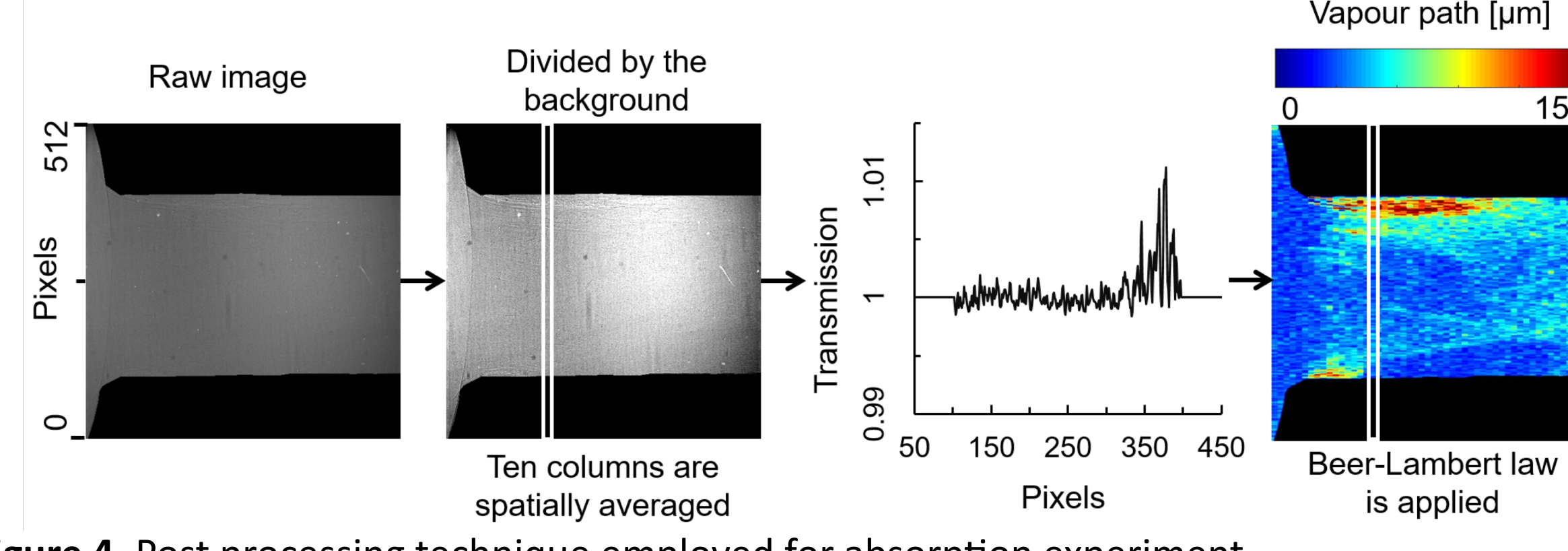


Figure 4. Post processing technique employed for absorption experiment.

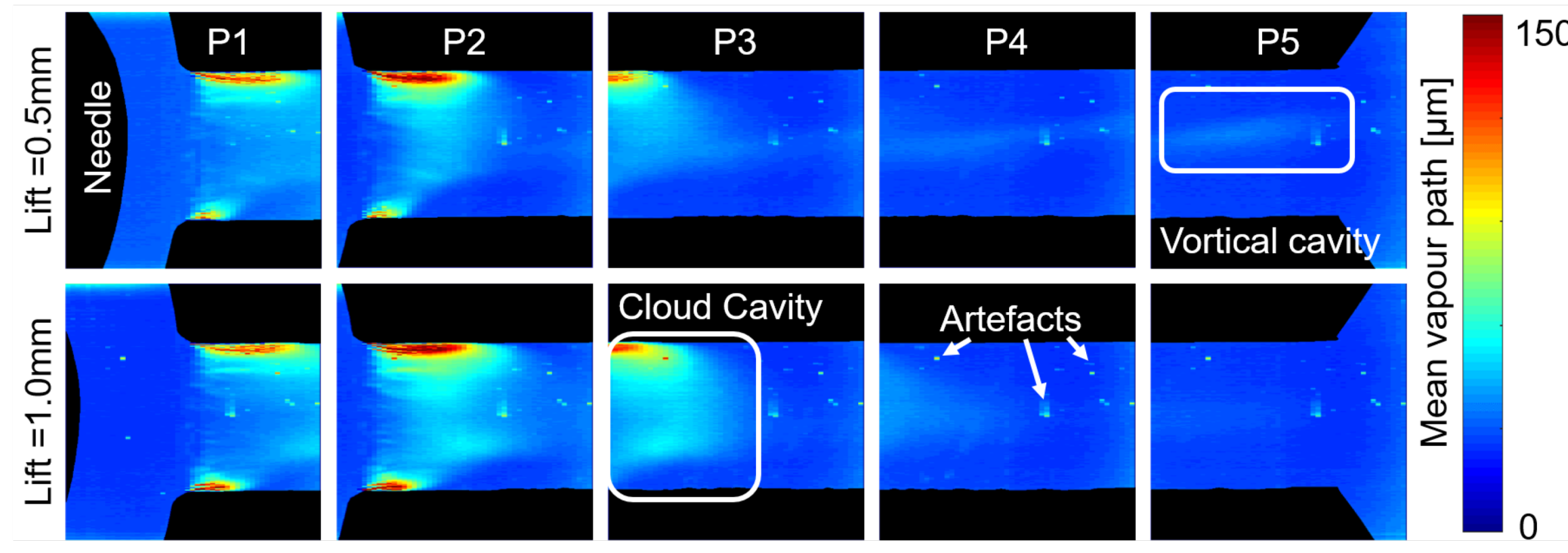


Figure 5. Contour plots of the mean vapour path along the line-of-sight dimension for CN=4.

2. Experimental setup

Diesel fuel was selected as the working fluid and circulated in a hydraulic flow loop under steady-state flow rate conditions where the prevailing flow conditions within the injector orifice were characterised with the use of Cavitation numbers in a range of 2 to 6, a Reynolds number equal to 35500 and two fixed needle lifts of 0.5 and 1.0 mm. The experimental campaign was conducted at the Advanced Photon Source in Argonne National Laboratory. A beam energy of 11.88 keV was selected to achieve the maximum contrast between liquid and vapour phases. The bunch of 8 septuplets with a 51 ns gap between groups was used in the present investigation where by using an appropriate combination of x-ray chopper/shutter, x-ray pulses at suitable frequencies to the given experiment was achieved. Subsequently, a 10 mm diameter crystal scintillator with a thickness of 0.1 mm was fitted to convert the x-ray beam to visible light after its interaction with the test section under investigation which was then captured by a charge-coupled device (CCD) sensor in a high speed camera at 67890 fps at an exposure time of 1μs to ‘freeze’ the highly transient nature of the two-phase flow inside the orifice. In an effort to increase the spatial resolution, the X-ray beam was collimated to a field of view of 2.56x2.56 mm discretized by 512x512 pixels resulting a 5 mm/pixel spatial resolution. As the orifice length (5 mm) was larger than the selected field of view, the overall length was segmented into five overlapping panels and each panel was irradiated successively as can be seen in Fig.1. An organic polymer (PEEK) was selected as the axisymmetric orifice material in order to have lower x-ray attenuation compared to metal orifices and a higher signal to noise ratio in comparison with the carbon fibre models used in previous studies of the authors [7,8].

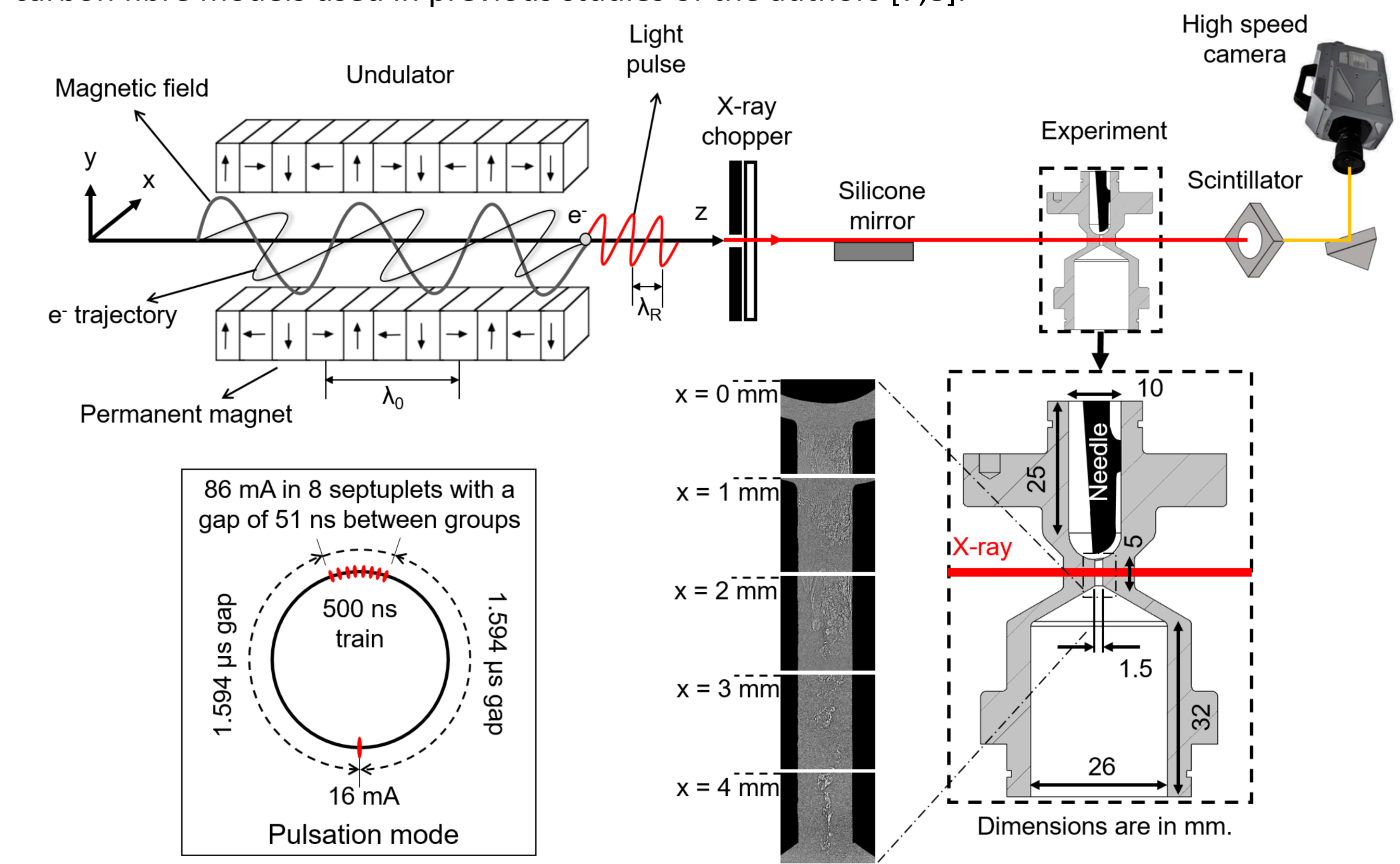


Figure 1. Schematic of the experimental setup for the x-ray imaging.

5. Discussion

XPCI is a powerful visualisation technique that can provide a faithful qualitative representation of highly perturbed and rapidly varying interfaces and also information on cavitation dynamics. However, it does not give any insight on the ‘depth’ of vapour structures. On the other hand, absorption technique can alleviate this limitation by illustrating the extent of vaporous structures along the line-of-sight dimension. Having said that, a concurrent consideration of both measurement techniques, can result in a three dimensional perception of the flow which is not conceivable using merely one of the utilised techniques. For instance, it can be deduced that at the orifice inlet, cavitation occurs in a ring shape encircling a vortical cavity that extends to the orifice exit. An illustrative example regarding potential pitfalls of qualitative techniques is given in Fig. 6, where results concerning both implemented techniques are shown. For instance, regarding the most complex cavitation topology arising in the examined cases ($L=1.0/CN=6.0$), the mean vapour probability is shown to be decreasing along the orifice length, while the vapour content values exhibit the opposite trend (Fig. 7). Hence, although in reality the vaporous structures gain in coherence along the line-of-sight dimension, an interpretation based on merely XPCI would suggest an opposite decaying trend.

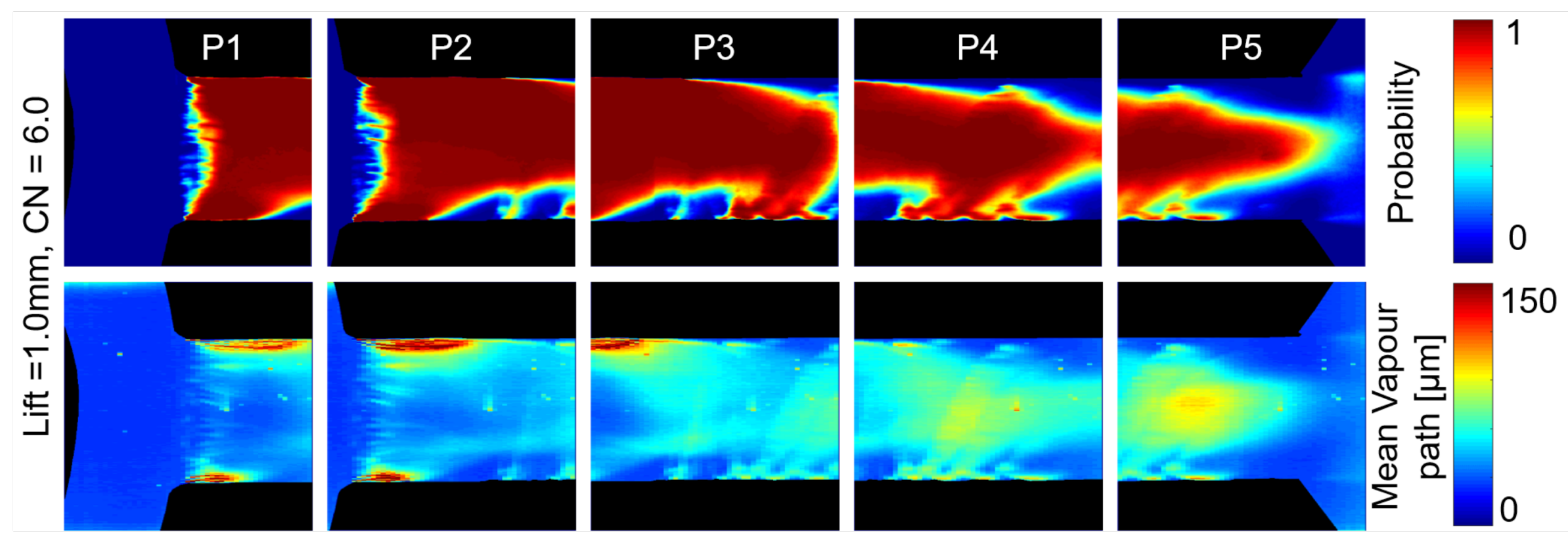


Figure 6. Contour plots of the time-averaged vapour probability and mean vapour path for $L=1/CN=6$.

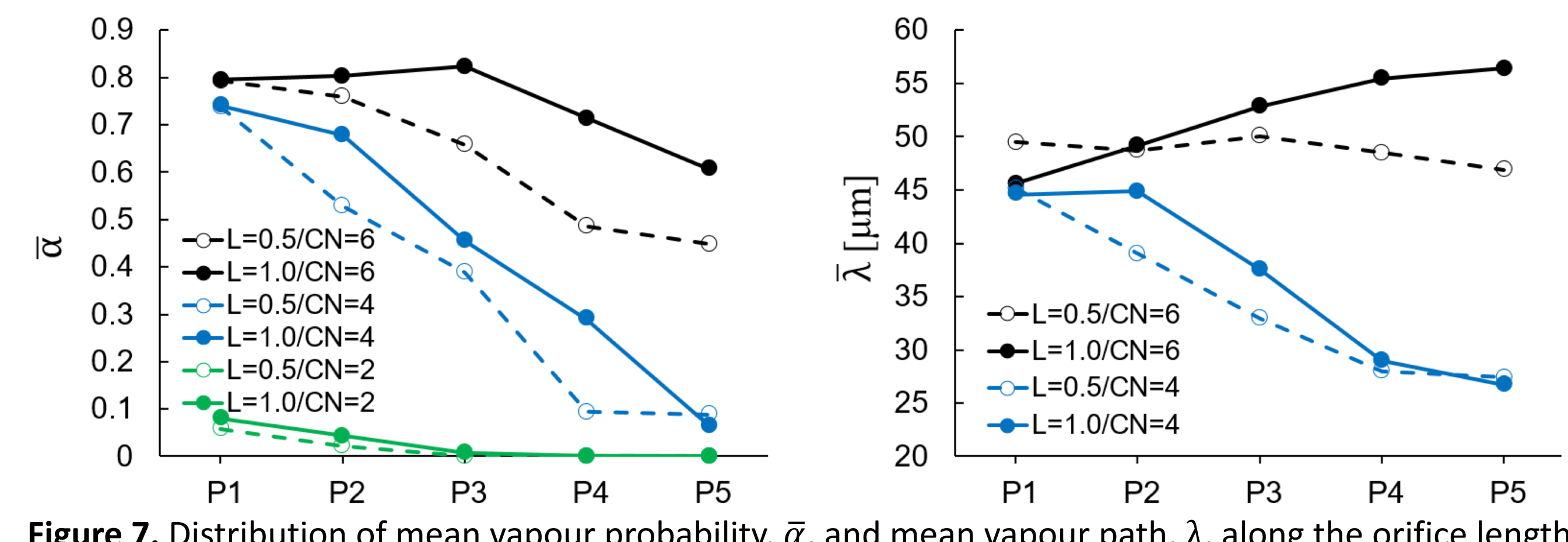


Figure 7. Distribution of mean vapour probability, $\bar{\alpha}$, and mean vapour path, $\bar{\lambda}$, along the orifice length.

Contact

Milad Heidari Koochi
City, University of London
Email: milad.Heidari-Koochi@city.ac.uk
Tel: +44(0)7397323562

References

- Kini, V., Bachmann, C., Fontaine, A., Deutscher, S., and Tarbell, J. M., 2000, "Flow Visualization in Mechanical Heart Valves: Occluder Rebound and Cavitation Potential," *Ann. Biomed. Eng.*, 28(4), pp. 431–441.
- Šarc, A., Kosej, J., Stopar, D., Oder, M., and Dular, M., 2018, "Removal of Bacteria *Legionella pneumophila*, *Escherichia coli*, and *Bacillus subtilis* by (Super)Cavitation," *Ultrason. Sonochem.*, 42(November 2017), pp. 228–236.
- Chan, W. K., 1990, "Correlation between Cavitation Type and Cavitation Erosion Centrifugal Pumps," *Int. J. Heat Fluid Flow*, 11(3), pp. 269–271.
- Escalar, X., Egusquiza, E., Farhat, M., Avellan, F., and Coussirat, M., 2006, "Detection of Cavitation in Hydraulic Turbines," *Mech. Syst. Signal Process.*, 20(4), pp. 983–1007.
- Arcoumanis, C., Flora, H., Gavaises, M., and Badami, M., 2000, "Cavitation in Real-Size Multi-Hole Diesel Injector Nozzles," *SAE Trans.*, 109, pp. 1485–1500.
- Ulas, A., 2006, "Passive Flow Control in Liquid-Propellant Rocket Engines with Cavitating Venturi," *Flow Meas. Instrum.*, 17(2), pp. 93–97.
- Karathanassis, I. K., Trickett, K., Koukouvinis, P., Wang, J., Barbour, R., and Gavaises, M., 2018, "Illustrating the Effect of Viscoelastic Additives on Cavitation and Turbulence with X-Ray Imaging," *Sci. Rep.*, 8(1), p. 14968.
- Karathanassis, I. K., Koukouvinis, P., Kontolatis, E., Lee, Z., Wang, J., Mitroglou, N., and Gavaises, M., 2018, "High-Speed Visualization of Vortical Cavitation Using Synchrotron Radiation," *J. Fluid Mech.*, 838, pp. 148–164.